First-ever model simulation of the new subclass of solitons "Supersolitons" in plasma

Amar Kakad,[a] Ajay Lotekar,[b] and Bharati Kakad[c]
Indian Institute of Geomagnetism, New Panvel, Navi Mumbai, India

"Supersolitons," the structures associated with the stationary solitary solutions with the Mach number greater than those associated with the double layers, were introduced in 2012. Later, many researchers have reported the existence domain of the supersolitons in different plasma constituents. However, their evolutionary dynamical behavior and stability were main concerns and were not yet explored. We performed fluid simulation of ion acoustic supersolitons in a plasma containing two-temperature electrons having kappa distributions in the presence of cold fluid ions. Our simulation shows that a specific form of the initial perturbation in the equilibrium electron and ion densities can evolve into ion acoustic supersolitons, which maintain their shape and size during their propagation. This is first-ever simulation to confirm the stability of the supersolitons that opens a new era in the field of solitary wave structures in space and laboratory plasmas. *Published by AIP Publishing.* [http://dx.doi.org/10.1063/1.4969078]

The concept of a new form of solitary waves, i.e., "super solitary waves," was proposed by Dubinov and Kolotkov.[1] Subsequently, several plasma models have been explored to show the existence/nonexistence of these structures in multi-component plasmas, which termed them as "supersolitons."[2–20] Supersolitons are characterized by having subsidiary extrema on the sides of a typical bipolar electric field signature or by association with the Mach numbers beyond the Mach number associated with double layer in the fully nonlinear Sagdeev pseudopotential description. This analysis is done in a stationary frame, which propagates with the solitary wave, for one mode at a time. This analysis gives solutions that represent stationary solitary waves, such as solitons, double layers, and supersolitons. The Sagdeev formalism cannot give time evolutionary information of both solitary and supersolitary structures. Hence, it excludes all discussion of the stability and interaction properties of the supersolitons. To address these issues, we carry out one-dimensional fluid simulations for one of the plasma models that support ion acoustic (IA) supersolitons.[3]

We consider a homogeneous unmagnetized plasma consisting of cold and hot electrons and cold positive fluid ions in a one-dimensional system.[3] The electrons are assumed as superthermal particles regulated by the kappa distribution function[21–25]

$$F(v_s) = \frac{n_{0s}}{\left(\pi \kappa_s \theta_s^2\right)^{1/2}} \frac{\Gamma(\kappa_s)}{\Gamma(\kappa_s - 1/2)} \left[1 + \frac{v_s^2}{\kappa_s \theta_s^2}\right]^{-\kappa_s}. \quad (1)$$

In the above equation, Γ is the gamma function, and n_{0s} and v_s are the density and velocity of the cold electrons ($s = ce$) and hot electrons ($s = he$). $\theta_s^2 = [(\kappa_s - 3/2)/\kappa_s]v_{th,s}^2$ is the

most probable speed, where $v_{th,s} = (2k_B T_s/m_s)^{1/2}$ is the thermal speed of the electrons, and k_B is the Boltzmann constant. T_s and m_s are temperature and mass of the electrons. The spectral index κ_s decides the slope of the tail of the distribution function, and it is always greater than 1.5. The cold and hot electron densities can be obtained by taking the first moment of Equation (1)

$$N_{ce} = f\left[1 - \frac{\Phi}{\tau(\kappa_{ce} - 3/2)}\right]^{-\kappa_{ce}+1/2}, \quad (2)$$

$$N_{he} = (1-f)\left[1 - \frac{\Phi}{(\kappa_{he} - 3/2)}\right]^{-\kappa_{he}+1/2}. \quad (3)$$

In the above equations, $f = n_{ce0}/n_{i0}$, $\tau = T_{ce}/T_{he}$, the densities of cold (n_{ce}) and hot (n_{he}) electrons are normalized as $N_{ce} = n_{ce}/n_{i0}$ and $N_{he} = n_{he}/n_{i0}$, respectively. The electrostatic potential (ϕ) is normalized as $\Phi = e\phi/k_B T_{he}$. The κ_{ce} and κ_{he} are the spectral indices associated with the cold and hot electrons, respectively.

The ions are governed by the fluid equations of continuity and momentum

$$\frac{\partial N_i}{\partial t_n} + \frac{\partial (N_i U_i)}{\partial x_n} = 0, \quad (4)$$

$$\frac{\partial U_i}{\partial t_n} + U_i \frac{\partial U_i}{\partial x_n} = -\frac{\partial \Phi}{\partial x_n}, \quad (5)$$

where N_i and U_i are normalized density and velocity of the ions in the x-direction, respectively. At the equilibrium state, the plasma follows quasi-neutrality, under which the ion density is equivalent to the electron density, i.e., $n_{i0} = n_{ce0} + n_{he0}$. Here, n_{ce0}, n_{he0}, and n_{i0}, respectively, are the cold electron density, hot electron density, and the ion density at the equilibrium. The electron and ion equations are coupled by the Poisson equation

---

[a] amar@iigs.iigm.res.in
[b] ablotekar@gmail.com
[c] ebharati@iigs.iigm.res.in

$$\frac{\partial^2 \Phi}{\partial x_n^2} = N_{ce} + N_{he} - N_i. \tag{6}$$

In the above equations, the ion fluid velocity v_i and the ion density n_i are normalized as $U_i = v_i/C_{IA}$ and $N_i = n_i/n_{i0}$, respectively. The space and time are normalized by the hot electron Debye length $\lambda_{Dhe} = (k_B T_{he} \epsilon_0 / n_{i0} e^2)^{1/2}$ and inverse of the ion plasma oscillation frequency $\omega_{pi}^{-1} = (\epsilon_0 m_i / n_{i0} e^2)^{1/2}$, respectively. It gives $x_n = x/\lambda_{Dhe}$ and $t_n = \omega_{pi} t$. The characteristic IA sound speed used in the velocity normalization is $C_{IA} = (k_B T_{he}/m_i)^{1/2}$.

We modified the one-dimensional fluid code of Lotekar et al.[25] for the plasma model considered in this paper. In this case, for the numerical solution of the set of Equations (4), (5), and (6), the system is fragmented into the equidistance grid points in space and time. All the plasma quantities are calculated on the grid points. In this discretized system, the first order differential operator is replaced by its corresponding difference formula. The spatial derivatives in Equations (4) and (5) are replaced by the fourth order central finite difference formula.[26–29] The time integration of Equations (4) and (5) is done by using the leap-frog method,[27] which is second order accurate in time. To remove the high-frequency errors introduced due to the spatial discretization, we use the compensating filter.[27] A necessary condition for the convergence of the explicit finite difference method used in our simulation is that it has constrained by the Courant condition, $U_{max} \Delta t / \Delta x \leq 1$. This condition states that for any given time-step (Δt), the maximum velocity in the system (U_{max}) must not be greater than that which would allow fluid to travel more than one grid-step (Δx). The Δx and Δt in our simulation are chosen in such a way that the Courant condition is always fulfilled.

In the simulation, initially, the background equilibrium densities of all three plasma constituents are superimposed by Gaussian type perturbation[25]

$$\delta n = \Delta n \, \exp \left[-\left(\frac{x - x_c}{l_0} \right)^2 \right]. \tag{7}$$

In the above equation, Δn is the amplitude of the perturbation, x is the position on the x-axis, x_c is the center of the system, and l_0 controls the width of the perturbation. We consider the initial density perturbation (IDP) with $\Delta n = 1.9$ n_{i0} and $l_0 = 10\lambda_{Dhe}$. We set the following parameter values in the simulation run: grid spacing: $\Delta x = 0.2 \, \lambda_{Dhe}$, time interval: $\Delta t = 0.1 \, \omega_{pi}^{-1}$, and system length: $L_x = 40,000\lambda_{Dhe}$. The fluid simulation was performed in a one-dimensional system with periodic boundary conditions. We performed simulation for the case of moderately superthermal electrons as discussed by Verheest et al.[3] The parameters considered in the simulation are $f = 0.055$, $\tau = 0.12$, $\kappa_{ce} = 10$, and $\kappa_{he} = 10$. The flow velocities of the plasma species at $t = 0$ are assumed to be zero.

We first undertake a discussion of the generation and evolution of IA supersolitons, when the long wavelength IDP is used to perturb the background electron and ion densities in the fluid simulation. The long wavelength IDP considered here is the same as that described in the study of Kakad et al.[28] The schematics of the different steps involved in the evolution of the IA supersolitons in terms of electrostatic potential (upper panels) and associated electric field (bottom panels) are shown in Figure 1. The quasi-neutrality at the equilibrium causes the electrostatic potential in the system to be zero. As cold and hot electrons follow the kappa distributions, it leads to the generation of the finite electrostatic potential at the first time step in the simulation system. The normalized electrostatic potential (Φ) and electric field (E_n) associated with it are shown at $\omega_{pi} t = 0.1$ in Figure 1(a). Here, t is a product of the number of simulation time steps and Δt. It is observed that the amplitude of the electrostatic potential in the system decreases with time. This decrease of the potential eventually stops after some time, and the pulse starts splitting from its top point through formation of the trough (not shown here). Once the value of the Φ approaches to zero at the centre of the trough, two identical solitary pulses in the potential and electric field are formed in the system. Further, these two pulses propagate with the speed V_s in a direction opposite to each other, i.e., towards the boundaries of the simulation system. Both pulses are
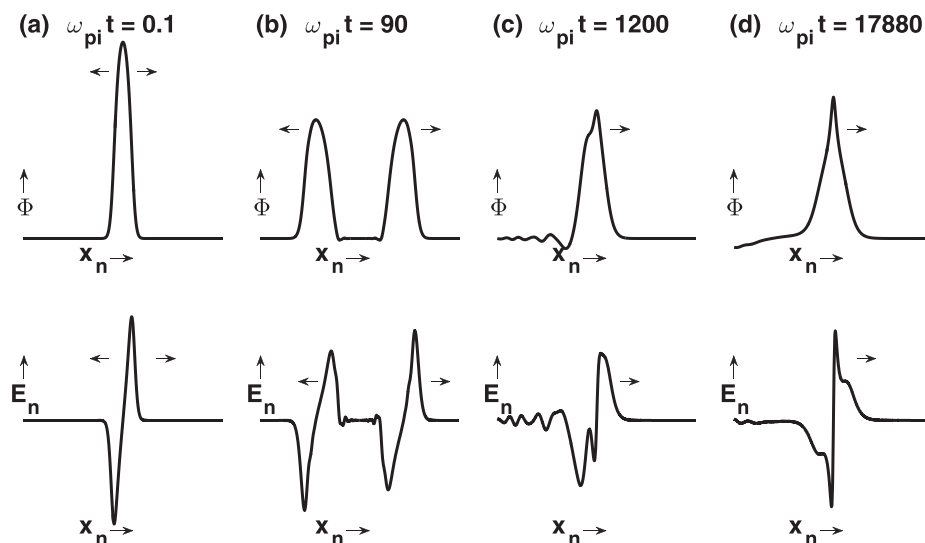
FIG. 1. Schematic diagrams illustrate some of the stages during formation of the IA supersolitons in the simulation.

identified as long wavelength ion acoustic solitary wave (IASW) pulses and are found to be weakly dispersive. One of the snapshots of these propagating pulses at $\omega_{pi}t = 90$ is shown in Figure 1(b). Later, during their propagation the amplitude and speed of IASW pulses gradually increase. Consequently, the trailing edges of both pulses tend to steepen with time. One of such pulses propagating towards the right-side boundary of the simulation system at $\omega_{pi}t = 1200$ is shown in Figure 1(c). In the course of steepening of the pulses, some oscillations are generated at the trailing edge of both pulses. These oscillations are identified as IA oscillations. The IA oscillations propagate with the speed, V_{s0}, such that the IA oscillations lag behind the IASW pulses (i.e., $V_{s0} < V_s$) with time. Because of the steepening, the amplitude and speed of the IASW pulse increase. Generally, the evolution of the long wavelength weakly dispersive IASW pulse can lead to its steepening followed by the wave breaking.[28,30] However, we observed a different process in the present simulation. The amplitude of the pulse increases because of steepening; however, the IASW pulse does not break in the simulation. Instead, the pulse becomes wider at the bottom-side. Subsequently, the IA oscillations detached from the trailing edge of the pulses after sufficiently long time and the stable supersoliton form in the system (see supplementary material for the evolution of supersoliton, which is created from the simulation data). One of the snapshots of the supersoliton pulse propagating towards the right-side boundary of the simulation system at time $\omega_{pi}t = 17,880$ is shown in Figure 1(d).

The dispersion characteristics of the evolving plasma system will help us to identify different wave modes supported by the plasma system. We have obtained the power spectrum from the Fourier transformation of the electrostatic potential over space and time. Figure 2 shows the power spectra of the potential (Φ) from the simulation run. These power spectra are taken over the period of $\omega_{pi}t = 0$–200. In this plot, the black and white dashed curves are plotted from the linear dispersion relations derived from Equations (4), (5), and (7). Among these two lines, the white dashed lines are plotted from the linear dispersion equation that is

obtained without considering the plasma approximation of the quasi-neutrality, i.e., $N_i \neq N_e$, which is given as

$$\omega^2 = \frac{k^2}{\left[k^2 + f\frac{(\kappa_{ce} - 1/2)}{\tau(\kappa_{ce} - 3/2)} + (1-f)\frac{(\kappa_{he} - 1/2)}{(\kappa_{he} - 3/2)}\right]}, \quad (8)$$

where ω is the frequency and k is the wave number. The dashed black line is from the linear dispersion equation with the consideration of the plasma approximation ($N_i = N_e$) and it reads as

$$\omega^2 = \frac{k^2}{\left[f\frac{(\kappa_{ce-}1/2)}{\tau(\kappa_{ce} - 3/2)} + (1-f)\frac{(\kappa_{he} - 1/2)}{(\kappa_{he} - 3/2)}\right]}. \quad (9)$$

In Figure 2, two types of dispersion curves are clearly visible. It is found that one dispersion curve follows the white line while another follows the dashed black line. The dispersion that follows the dashed white line is diagnosed as nondispersive IA supersoliton pulses, which propagate with constant wave speed. The other dispersion that follows the dashed black line is identified as the dispersive IA oscillations.

We examine the evolution and propagation of different wave structures through spatial and temporal evolution of their electrostatic potentials, which is depicted in Figure 3. In Figure 3, we show only part of the simulation system, i.e., from $L_x - x_c = -6000$ to $6000\lambda_{Dhe}$ for the simulation run. In this plot, $x - x_c = 0$ represents the center of the simulation system at which the IDP is introduced at $\omega_{pi}t = 0$. Figure 3 shows two identical sets of band structures that represent the IASW pulses and the IA oscillations propagating along both positive and negative x–directions. The small window at the center of the plot shows the magnified image, where some region of the IA waves propagating in the positive x–direction is illustrated. The amplitude of the electric field associated with the IASW pulses in the system is higher as compared to that of the IA oscillations. Therefore, the dark red bands in Figure 3 represent the IASW pulses, whereas the alternate blue yellow and light blue bands represent the IA oscillations. The inverse of the slope of the red bands in Figure 3 gives the speed of the IA supersolitons. The positive
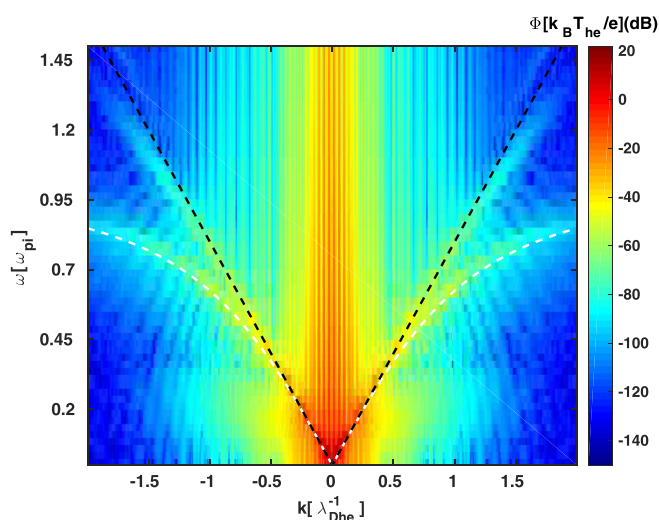
FIG. 2. ω-k diagram during $\omega_{pi}t = 0$–200 from the simulation.
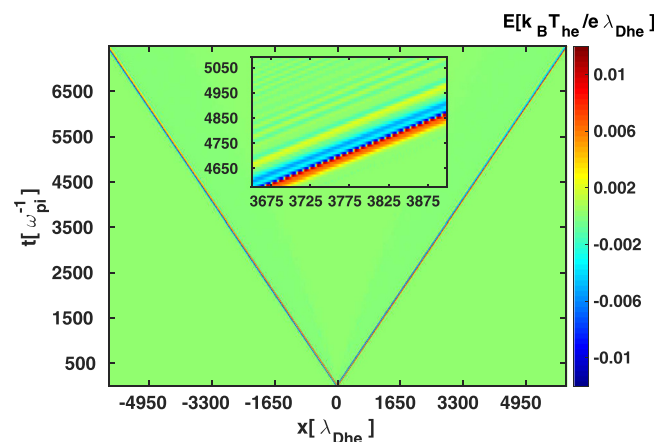
FIG. 3. Spatio-temporal evolution of the electric field in the simulation.
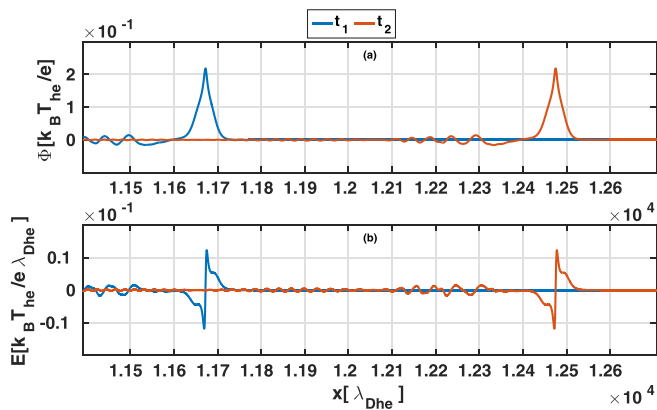
FIG. 4. Snapshots of the (a) potential and (b) electric field associated with the IA supersoliton at $\omega_{pi}t_1 = 14{,}550$ (blue curve) and $\omega_{pi}t_2 = 15{,}550$ (red curve) from the simulation.

(negative) value of the inverse of the slope indicates the IA supersoliton pulse propagating in the positive (negative) x–direction.

To demonstrate the stability of the IA supersolitons, we have shown snapshots of the supersolitons propagating in the positive x–direction at $\omega_{pi}t_1 = 14{,}550$ and $\omega_{pi}t_2 = 15{,}550$ in Figure 4. The snapshots at two different times show that the amplitude of the potential and electric field associated with each supersoliton is nearly the same, which reveals the stability of the supersolitons in the system.

We compare the supersoliton profile from the simulation with the profile obtained from the nonlinear fluid theory.[3] For this, we obtained the speed (i.e., Mach number) of the supersoliton in the stability region as suggested in Figure 4. We observed that the supersoliton characteristics are unchanged between $\omega_{pi}t = 14{,}100$ and $16{,}100$. We obtained the speed of the supersoliton in this stability region from its spatial and temporal variation as shown in Figure 3. The normalized speed (i.e., Mach Number, M) of the supersoliton obtained from the simulation is 0.80294. We used this speed in the energy integral equation, i.e., Equation (5) of Verheest et al.[3] to obtain the supersoliton profile from their model. Figure 5 shows the comparison of the profiles of the (a) electrostatic potential and (b) associated bipolar electric field of the IA supersolitons obtained from theory with those in the simulation (at $\omega_{pi}t = 16{,}000$). The amplitude and width of the supersolitons from the simulation are 0.2182 and 28.14,
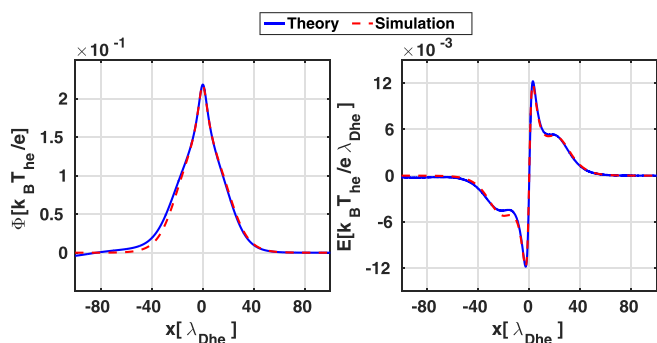
FIG. 5. The (a) potential (Φ) and (b) electric field (E_n) profiles of the IA supersoliton from the simulation and theory.

respectively, whereas the amplitude and width from the theory are found to be 0.2178 and 29.19, respectively. This shows that both potential and electric field associated with the supersolitons obtained from theory and simulation are comparable.

In conclusion, we report the first-ever computer simulation of the evolution of IA supersolitons in the plasma composed of cold and hot superthermal electrons and cold fluid ions. We found that the specific form of perturbation in the equilibrium densities of the plasma constituents evolved into the IA supersolitons. The generated ion acoustic supersolitons in the simulation are longitudinal density perturbations, driven by electric field that arises from the space charge developed by the slight displacements between the ion and electron due to the density perturbations. The speed, amplitude, and width of these structures depend on the perturbation parameters, the electron temperature ratio (τ), and density ratio (f) considered in the simulation. This simulation has made it possible to follow the detailed evolution of IA supersolitons and its stability over few thousands of ω_{pi} in the plasma.

The presence of plasma constituents and the form of IDP in the simulation both decide whether the pair of solitons or chains of solitons or supersolitons will be evolved. For the plasma model considered in this paper, all three types of structures are possible with different IDP forms (i.e., with different widths and amplitudes). In this paper, we have presented evolution of the specific form of the IDP that evolves as only supersolitons. However, why this IDP evolves into pair of supersolitons and not into chain of IA solitons needs to be understood. In the evolution of supersoliton, it is seen that the amplitude of the initially developed IASW pulse increases because of the steepening; however, this pulse do not break. Instead, the pulse becomes wider at the bottom-side and evolved as a supersoliton. This indicates that the nonlinearity and the dispersion got balanced to maintain the shape and size of the supersoliton structures in the system, before reaching at the critical amplitude required for the wave breaking.

Recently, there has been a great deal of interest in the study of supersoliton structures. In these studies, the nonlinear fluid theory of the standard arbitrary amplitude solitons has allowed researchers to discover characteristics of the supersolitons in different plasma constituents. These theories have shown that the supersolitons are characterized by subsidiary extrema on the sides of a typical bipolar electric field signature or by association with a Mach number beyond double layers' Mach number. The potential profiles of supersolitons superficially look like those of traditional solitons. However, its close view shows two small bulges at both sides of the potential pulse of the supersoliton. Our fluid simulation also shows the same features of supersolitons as predicted by the fully nonlinear Sagdeev pseudopotential description. The width, amplitude, and speed of the IA supersolitons obtained from the simulations are comparable with those obtained from the theory.

The IA solitons, electron acoustic solitons, IA double layers, and electron acoustic double layers constitute a subclass of nonlinear electrostatic modes in the fluid description

of the plasma. These structures are found under laboratory conditions in current carrying and voltage driven plasmas as well as in plasmas driven by beam particle injection or by wave launching. Experimental evidence is furthermore provided by observations in the boundary layer regions of the Earth's magnetosphere.[31,32] With confirmation of the formation and stability of the supersolitons in the simulation, we proposed that the IA supersolitons are part of the subclass of nonlinear electrostatic modes. This has open up new questions as: whether supersolitons exist in kinetic description? If so, how different will be the dynamics of the hump/hole associated with the supersoliton in comparison with the regular hump/hole in the plasma? Whether hole/hump associated with the supersolitons will transport/accelerate more charge particles than the usual hump/hole in the plasma? Do supersoliton type structures exist in space and laboratory plasmas? In conclusion, the simulation of supersolitons has opened a new era in the field of solitary wave structures in space and laboratory plasmas.

See supplementary material for the animation of the evolution of supersolitons, which is created from the simulation data. In this animation, we have shown one of the supersolitons propagating toward the right-side boundary of the simulation system.

[1]A. Dubinov and D. Y. Kolotkov, Plasma Phys. Rep. **38**, 909 (2012).
[2]F. Verheest, M. A. Hellberg, and I. Kourakis, Phys. Plasmas **20**, 012302 (2013).
[3]F. Verheest, M. A. Hellberg, and I. Kourakis, Phys. Plasmas **20**, 082309 (2013).
[4]F. Verheest and M. A. Hellberg, Phys. Plasmas **22**, 012301 (2015).
[5]O. Rufai, R. Bharuthram, S. Singh, and G. Lakhina, Phys. Plasmas **21**, 082304 (2014).
[6]G. Lakhina, S. Singh, and A. Kakad, Phys. Plasmas **21**, 062311 (2014).
[7]S. Ghosh and A. S. Iyengar, Phys. Plasmas **21**, 082104 (2014).
[8]S. Singh and G. Lakhina, Commun. Nonlinear Sci. Numer. Simul. **23**, 274 (2015).
[9]C. Olivier, S. Maharaj, and R. Bharuthram, Phys. Plasmas **22**, 082312 (2015).
[10]O. Rufai, Phys. Plasmas **22**, 052309 (2015).
[11]O. Rufai, R. Bharuthram, S. Singh, and G. Lakhina, Phys. Plasmas **22**, 102305 (2015).
[12]S. S. Varghese and S. Ghosh, Phys. Plasmas **23**, 082304 (2016).
[13]O. Rufai, R. Bharuthram, S. Singh, and G. Lakhina, Adv. Space Res. **57**, 813 (2016).
[14]F. Verheest, Phys. Plasmas **18**, 083701 (2011).
[15]T. K. Baluku, M. A. Hellberg, and F. Verheest, Europhys. Lett. **91**, 15001 (2010).
[16]A. E. Dubinov and D. Y. Kolotkov, IEEE Trans. Plasma Sci. **40**, 1429 (2012).
[17]F. Verheest, M. A. Hellberg, and I. Kourakis, Phys. Rev. E **87**, 043107 (2013).
[18]F. Verheest, J. Plasma Phys. **80**, 787 (2014).
[19]S. Maharaj, R. Bharuthram, S. Singh, and G. Lakhina, Phys. Plasmas **20**, 083705 (2013).
[20]M. A. Hellberg, T. K. Baluku, F. Verheest, and I. Kourakis, J. Plasma Phys. **79**, 1039 (2013).
[21]M. Hellberg, R. Mace, T. Baluku, I. Kourakis, and N. Saini, Phys. Plasmas **16**, 094701 (2009).
[22]I. Kourakis, S. Sultana, and M. Hellberg, Plasma Phys. Controlled Fusion **54**, 124001 (2012).
[23]G. Livadiotis and D. McComas, Space Sci. Rev. **175**, 183 (2013).
[24]G. Livadiotis, J. Geophys. Res.: Space Phys. **120**, 1607, doi:10.1002/2014JA020825 (2015).
[25]A. Lotekar, A. Kakad, and B. Kakad, Phys. Plasmas **23**, 102108 (2016).
[26]K. Watanabe and T. Sato, Computer Space Plasma Physics: Simulation Techniques and Software (Terra Scientific, Tokyo Japan, 1993), p. 209.
[27]Y. Omura and J. L. Green, J. Geophys. Res.: Space Phys. **98**, 9189, doi:10.1029/92JA02901 (1993).
[28]A. Kakad, Y. Omura, and B. Kakad, Phys. Plasmas **20**, 062103 (2013).
[29]B. Kakad, A. Kakad, and Y. Omura, J. Geophys. Res.: Space Phys. **119**, 5589, doi:10.1002/2014JA019798 (2014).
[30]A. Kakad and B. Kakad, "Ponderomotive processes as proxies for breaking of ion acoustic solitary waves," Phys. Plasmas (to be published).
[31]J. Pickett, L.-J. Chen, S. Kahler, O. Santolik, D. Gurnett, B. Tsurutani, and A. Balogh, Ann. Geophys. **22**, 2515–2523 (2004).
[32]A. Kakad, B. Kakad, C. Anekallu, G. Lakhina, Y. Omura, and A. Fazakerley, J. Geophys. Res.: Space Phys. **121**, 4452–4465, doi:10.1002/2016JA022365 (2016).